AAS 14-201

A BOUNDARY VALUE PROBLEM APPROACH TO TOO-SHORT ARC OPTICAL TRACK ASSOCIATION

K. Fujimoto[*], K. T. Alfriend[†], and T. Schildknecht[‡]

Given a short-arc optical observation with estimated angle-rates, the admissible region is a compact region in the range / range-rate space defined such that all likely and relevant orbits are contained within it. An alternative boundary value problem formulation has recently been proposed where range / range hypotheses are generated with two angle measurements from two tracks as input. In this paper, angle-rate information is reintroduced as a means to eliminate hypotheses by bounding their constants of motion before a more computationally costly Lambert solver or differential correction algorithm is run.

INTRODUCTION

One problem of concern in space situational awareness (SSA) is the association of observations of resident space objects (RSOs) and the initial determination of their orbits thereafter. Due to the vastly larger number of RSOs compared to sensors, only a limited number of observations are available per night per object, each over observation arcs that can be as short as a few seconds. Therefore, a single track, regardless of measurement type, often does not contain sufficient information in order to reliably estimate the observed object's state or conduct follow-up observations. Traditional association methods, then, can perform poorly as they often rely upon the quality of the orbit determination solution to determine associations. This dependency of the association on the initial orbit determination (IOD) and vice versa is at the crux of the so called too-short arc (TSA) problem.

The admissible region (AR) approach has been studied in recent years as one solution technique [1–8]. Given a short-arc series of optical measurements, or a tracklet, the angle and angle-rate at epoch is estimated, most commonly by a least-squares fit to a polynomial kinematic model. A compact region in the range / range-rate space is defined based on a set of physical constraints such that all likely and relevant orbits are contained within it [9–11]. In this initial value problem interpretation, each point in the admissible region, combined with the angular variables, corresponds to a hypothesis of the full 6-dimensional state that the observed object may have taken. Since two variables are unknown per observation, only two tracklets are required for association and subsequent state estimation instead of three for geometric IOD. Therefore, many branches of the combinatorial tree structure of observations may be eliminated in runtime $O(mn^2)$, where n is the total number

[*]Postdoctorate research assistant, Department of Aerospace Engineering, Texas A&M University, 431 UCB ECEE 166 Boulder, CO 80309-0431

[†]TEES Distinguished Research Chair Professor, Department of Aerospace Engineering, Texas A&M University, H. R. Bright Bldg. Room 701 3141 TAMU College Station, TX 77843-3141

[‡]Professor, Astronomical Institute, University of Bern, Sidlerstrasse 5 CH-3012 Bern, Switzerland

of tracklets to be associated and m is the number of range / range-rate hypotheses made per tracklet pair, before running the full problem of associating three or more tracklets. With potentially thousands of tracklets gathered every night, an AR-like approach can end up being more computationally efficient overall than conventional techniques even though it may be slower per individual association run [12].

For extremely short tracklets spanning $\sim 10^0$ seconds, however, the angle-rates are so poorly determined that both false positive and negative association outcomes become prevalent. As such, an alternative boundary value problem (BVP) formulation of the AR has been proposed by Schumacher et al., where range / range hypotheses are generated and then evaluated by ultimately solving Lambert's problem with two angle measurements from two tracklets as input [12]. A similar approach is introduced earlier by Virtanen, et al. in the context of short-arc IOD for heliocentric objects, but in their work, the range bounds are not rigorously defined [13]. Indeed, in Schumacher, et al., many range / range hypotheses are found to be eliminated based on orbital element bounds as well as special closed-form solutions to Lambert's problem. Siminski, et al. have also discussed benefits of a BVP AR formulation in the context of tracklet association and IOD posed as an optimization problem [14]. In this paper, angle-rate information is reintroduced in the BVP AR formulation but not as a state variable of the hypothesized objects; rather, it is used as a means to bound their constants of motion. These bounds further eliminate solutions before a more computationally costly Lambert solver or differential correction algorithm is run even when the angle-rate estimates are poor. Hypothesis gating has been discussed for the original initial value problem (IVP) formulation of the AR by Gadaleta, et al [15], but their technique is not directly applicable for the BVP formulation as it requires the propagation of attributable orbital elements and their associated uncertainties, which, in turn, would involve a Lambert solver.

The outline of the paper is as follows. Both the IVP and BVP formulations of the AR are first introduced (*The Range / Range Admissible Region*). Next, the proposed criteria for the constants of motion are developed along with analyses of how errors in the tracklet variables map to them (*Method*). Finally, these criteria are tested with simulated optical observations (*Results*) of medium Earth (MEO), high Earth (HEO), and geosynchronous orbit (GEO) objects. The proposed criteria succeeds in eliminating over 30% of possible tracklet pairs as unassociated even before conducting a Lambert solver based IOD. The use of angular-rate data, with their potentially large errors taken into account, improves the computational viability of the BVP formulation of IOD via ARs, especially for extremely short arcs.

THE RANGE / RANGE ADMISSIBLE REGION

In the IVP formulation of the AR, for some tracklet, each range ρ / range-rate $\dot{\rho}$ hypothesis completes a full 6-dimensional kinematic state. That is, given tracklet $(\alpha_1, \delta_1, \dot{\alpha}_1, \dot{\delta}_1)$ in terms of right ascension α, declination δ, and their time derivatives at time t_1, and a hypothesis $(\rho_1, \dot{\rho}_1)$ associated with this tracklet, the position $\mathbf{r}_1$ and velocity $\dot{\mathbf{r}}_1$ are fully defined

$$\mathbf{r}_1 = \rho_1[\cos\alpha_1 \cos\delta_1, \sin\alpha_1 \cos\delta_1, \sin\delta_1] \tag{1}$$

$$\begin{aligned}\dot{\mathbf{r}}_1 = \dot{\rho}_1[\cos\alpha_1 \cos\delta_1, \sin\alpha_1 \cos\delta_1, \sin\delta_1] + \rho_1\dot{\alpha}_1[-\sin\alpha_1 \cos\delta_1, \cos\alpha_1 \cos\delta_1, 0] \\ + \rho_1\dot{\delta}_1[-\cos\alpha_1 \sin\delta_1, -\sin\alpha_1 \sin\delta_1, \cos\delta_1]\end{aligned} \tag{2}$$

Then, based on some equations of motion (EoM)

$$\ddot{\mathbf{r}} = f(\mathbf{r}, \dot{\mathbf{r}}, t), \tag{3}$$

the position $\mathbf{r}(t)$ and velocity $\dot{\mathbf{r}}(t)$ for any arbitrary time t may be solved for with $\mathbf{r}(t_1) = \mathbf{r}_1$ and $\dot{\mathbf{r}}(t_1) = \dot{\mathbf{r}}_1$ as initial conditions. Any range / range-rate hypothesis set for any given tracklet uniquely defines an orbit, but not all such orbits are feasible, likely, or relevant. Those that are lie in a compact region (i.e., the AR) defined in the range / range-rate space based on a set of physical criteria. The criteria may directly bound the hypothesized variables, the orbital energy, the periapsis or apoapsis, or orbital elements of the objects to be observed, and may also reflect the limitations to observational capabilities or the type of objects of interest to the analyst.

In the BVP formulation, a set of range values associated with two separate tracklets is hypothesized instead of range and range-rate for a single tracklet. Given tracklet $(\alpha_2, \delta_2, \dot{\alpha}_2, \dot{\delta}_2)$ at time t_2 in addition to the tracklet at time t_1, positions $\mathbf{r}_1$ and $\mathbf{r}_2$ are fully defined for range / range hypothesis set (ρ_1, ρ_2); $\mathbf{r}(t)$ and $\dot{\mathbf{r}}(t)$ may again be solved for based on eq. (3). The BVP under two-body dynamics is better known as Lambert's problem, for which many solution techniques exist [16]. In Schumacher et al., the criteria which define the AR are based on bounds on the Keplerian orbital elements of the observed object [12]

$$a \in [a_{\mathrm{MIN}}, a_{\mathrm{MAX}}], e \in [e_{\mathrm{MIN}}, e_{\mathrm{MAX}}], i \in [i_{\mathrm{MIN}}, i_{\mathrm{MAX}}]. \tag{4}$$

Bounds may further be defined for the right ascension of the ascending node Ω, but such bounds are inapplicable for most survey-like observation strategies and thus are ignored in this paper. The semi-major axis and eccentricity element bounds geometrically constrain the minimum perigee and maximum apogee

$$a_{\mathrm{MIN}}(1 - e_{\mathrm{MAX}}) \leq \|\mathbf{r}\| \leq a_{\mathrm{MAX}}(1 + e_{\mathrm{MAX}}), \tag{5}$$

which can be transformed into range bounds for either range value in the hypothesis set as

$$\rho \geq -(\mathbf{R} \cdot \mathbf{u}) + \sqrt{(\mathbf{R} \cdot \mathbf{u})^2 + [a_{\mathrm{MIN}}^2(1 - e_{\mathrm{MAX}})^2 - \mathbf{R} \cdot \mathbf{R}]} \tag{6}$$

$$0 \leq \rho \leq -(\mathbf{R} \cdot \mathbf{u}) + \sqrt{(\mathbf{R} \cdot \mathbf{u})^2 + [a_{\mathrm{MAX}}^2(1 + e_{\mathrm{MAX}})^2 - \mathbf{R} \cdot \mathbf{R}]}, \tag{7}$$

where $\mathbf{R}$ is the position of the observer, $\mathbf{u}$ is the unit vector along the range direction of the observation, and an Earth-based observer is assumed. Similarly, from the inclination bounds,

$$\mathbf{n} = \pm \frac{\mathbf{r}_1 \times \mathbf{r}_2}{\|\mathbf{r}_1 \times \mathbf{r}_2\|} \tag{8}$$

$$\cos i_{\mathrm{MAX}} \leq \mathbf{n} \cdot \mathbf{k} \leq \cos i_{\mathrm{MIN}}, \tag{9}$$

where $\mathbf{k}$ is a unit vector in the Z-direction in the Earth centered inertial frame. Next, constraints on range may be derived based on special solutions to Lambert's problem. Namely, the minimum possible semi-major axis a_0 and eccentricity e_0 solutions are given as [17]

$$a_0 = \frac{\|\mathbf{r}_1\| + \|\mathbf{r}_2\| + \|\mathbf{r}_2 - \mathbf{r}_1\|}{4} \tag{10}$$

$$e_0 = \frac{|\,\|\mathbf{r}_1\| - \|\mathbf{r}_2\|\,|}{\|\mathbf{r}_1 - \mathbf{r}_2\|}. \tag{11}$$

From the orbital element bounds, $a_0 \leq a_{\mathrm{MAX}}$ and $e_0 \leq e_{\mathrm{MAX}}$ are required. Finally, the lower

bound (i.e., parabolic) time of flight Δt_p is given as

$$\lambda = \sqrt{\frac{\|\mathbf{r}_1\| + \|\mathbf{r}_2\| - \|\mathbf{r}_2 - \mathbf{r}_1\|}{\|\mathbf{r}_1\| + \|\mathbf{r}_2\| + \|\mathbf{r}_2 - \mathbf{r}_1\|}} \tag{12}$$

$$\Delta t_p = \frac{4}{3}\sqrt{\frac{a_0^3}{\mu}}(1 - s\lambda^3), \tag{13}$$

where $s = \pm 1$ depending on the short- or long-way solution and μ is the standard gravitational parameter. Consequently, $\Delta t_p \leq (t_2 - t_1)$ is required.

METHOD

In this section, three additional criteria are introduced to eliminate range / range hypotheses based on both angles and angle-rates data from the tracklet, the latter potentially being poor. The inclusion of angle-rates allows for the use of constants of motion to eliminate hypotheses, namely: **1.** whether the minimum possible orbital energy meets semi-major axis bounds, **2.** whether the minimum possible angular momentum magnitude meets eccentricity bounds, and **3.** whether the angular momentum direction is consistent with the observed angle-rates. The deterministic bounds are first derived. Then, the map from the errors in the observed variables to the constants of motion is characterized and subsequently incorporated in the association process.

Energy Bound

The orbital energy $\mathcal{E}$ of an object in terms of topocentric spherical coordinates is given as

$$2\mathcal{E} = \dot{\rho}^2 + w_1\dot{\rho} + F(\rho), \tag{14}$$

where coefficient w_1 is determined by the input parameters (namely, the tracklet angles, angle-rates, and the observer location) and $F(\rho)$ is a function of the range and input parameters. Since range is hypothesized and may be assumed as known, if semi-major axis bounds $[a_{\mathrm{MIN}}, a_{\mathrm{MAX}}]$ are specified and if the quadratic equation with respect to range-rate

$$2\mathcal{E}_{\mathrm{MAX}} = 2\left[-\frac{\mu}{2a_{\mathrm{MAX}}}\right] = \dot{\rho}^2 + w_1\dot{\rho} + F(\rho) \tag{15}$$

does not have a real solution, the range hypothesis cannot be true. Note that it is not necessary to check the case for a_{MIN} as

$$-\frac{\mu}{2a_{\mathrm{MIN}}} \leq -\frac{\mu}{2a_{\mathrm{MAX}}} \tag{16}$$

for $a_{\mathrm{MIN}} > 0$, $a_{\mathrm{MAX}} > 0$.

If the discriminant $\mathcal{D}$ of eq. (15) is negative, then no real solutions for range-rate exist for the particular range hypothesis chosen. This inequality would, in turn, bound range hypotheses, but large angle-rate errors would potentially change the sign of $\mathcal{D}$. Thus, one must determine how observational errors map into the discriminant. The first-order Taylor series expansion of this map is examined in this paper because a linear map will allow one to carry over a Gaussian assumption of the observed variables into the discriminant. That is, for an observation covariance matrix R, the variance $\sigma_{\mathcal{D}}^2$ of the discriminant is then computed as

$$\sigma_{\mathcal{D}}^2 = \left[\frac{\partial \mathcal{D}}{\partial \mathfrak{X}}\right] R \left[\frac{\partial \mathcal{D}}{\partial \mathfrak{X}}\right]^{\mathrm{T}}, \tag{17}$$

where $\mathfrak{X} = (\alpha, \delta, \dot{\alpha}, \dot{\delta})$ are the tracklet variables. The criterion for range hypotheses consistent with energy bounds may be modified so that, if

$$\mathcal{D} + n_{\mathcal{D}}\sigma_{\mathcal{D}} < 0, \tag{18}$$

then the range hypothesis is eliminated with some level of confidence specified by $n_{\mathcal{D}}$. $\mathcal{D}$ is concave down as a function of range

$$\begin{aligned}\mathcal{D} = -4[\dot{\alpha}^2\cos^2\delta + \dot{\delta}^2]\rho^2 - 4[2\dot{\alpha}\left(-\dot{q}_1\sin\alpha\cos\delta + \dot{q}_2\cos\alpha\cos\delta\right) \\ + 2\dot{\delta}\left(-\dot{q}_1\cos\alpha\sin\delta - \dot{q}_2\sin\alpha\sin\delta + \dot{q}_3\cos\delta\right)]\rho - 4\dot{q}_1^2 - 4\dot{q}_2^2 - 4\dot{q}_3^2 \\ + \frac{8\mu}{\sqrt{\rho^2 + \rho\left(2q_1\cos\alpha\cos\delta + 2q_2\sin\alpha\cos\delta + 2q_3\sin\delta\right) + {\mathrm{r_E}}^2}} + 8\mathcal{E}_{\mathrm{MAX}} \\ + \left(2\dot{q}_1\cos\alpha\cos\delta + 2\dot{q}_2\sin\alpha\cos\delta + 2\dot{q}_3\sin\delta\right)^2,\end{aligned} \tag{19}$$

where $\mathbf{q} = (q_1, q_2, q_3)$ is the observer location and $\dot{\mathbf{q}} = (\dot{q}_1, \dot{q}_2, \dot{q}_3)$ is the observer velocity. Viewed as a function of the angle-rates, $\mathcal{D}$ is similarly a concave down quadratic polynomial with maxima located at

$$\dot{\alpha}_{\mathcal{D},\mathrm{MAX}} = -\frac{\dot{q}_2\cos\alpha - \dot{q}_1\sin\alpha}{\rho\cos\delta} \tag{20}$$

$$\dot{\delta}_{\mathcal{D},\mathrm{MAX}} = \frac{\sin\delta(\dot{q}_1\cos\alpha + \dot{q}_2\sin\alpha)}{\rho}, \tag{21}$$

respectively. Next, taking partial derivatives,

$$\begin{aligned}\frac{\partial\mathcal{D}}{\partial\alpha} = -4[2\dot{\alpha}(-\dot{q}_1\cos\alpha\cos\delta - \dot{q}_2\sin\alpha\cos\delta) + 2\dot{\delta}(\dot{q}_1\sin\alpha\sin\delta - \dot{q}_2\cos\alpha\sin\delta)]\rho \\ - \frac{4\mu\rho(-2q_1\sin\alpha\cos\delta + 2q_2\cos\alpha\cos\delta)}{[\rho^2 + \rho(2q_1\cos\alpha\cos\delta + 2q_2\sin\alpha\cos\delta + 2q_3\sin\delta) + {\mathrm{r_E}}^2]^{3/2}} \\ + 2(2\dot{q}_1\cos\alpha\cos\delta + 2\dot{q}_2\sin\alpha\cos\delta + 2\dot{q}_3\sin\delta)(2\dot{q}_2\cos\alpha\cos\delta - 2\dot{q}_1\sin\alpha\cos\delta)\end{aligned} \tag{22}$$

$$\begin{aligned}\frac{\partial\mathcal{D}}{\partial\delta} = 8\dot{\alpha}^2\rho^2\cos\delta\sin\delta + 8\dot{q}_1\dot{\delta}\rho\cos\alpha\cos\delta + 8\dot{q}_2\dot{\delta}\rho\sin\alpha\cos\delta + 8\dot{q}_2\dot{\alpha}\rho\cos\alpha\sin\delta \\ - 8\dot{q}_1\dot{\alpha}\rho\sin\delta\sin\alpha + \frac{8\mu\left(q_1\rho\cos\alpha\sin\delta + q_2\rho\sin\delta\sin\alpha - q_3\rho\cos\delta\right)}{\left(2q_1\rho\cos\alpha\cos\delta + 2q_2\rho\cos\delta\sin\alpha + 2q_3\rho\sin\delta + {\mathrm{r_E}}^2 + \rho^2\right)^{3/2}} \\ - 8\dot{q}_1^2\cos^2\alpha\cos\delta\sin\delta - 16\dot{q}_1\dot{q}_2\cos\alpha\cos\delta\sin\alpha\sin\delta - 8\dot{q}_2^2\cos\delta\sin^2\alpha\sin\delta\end{aligned} \tag{23}$$

$$\frac{\partial\mathcal{D}}{\partial\dot{\alpha}} = -8\dot{\alpha}\rho^2\cos^2\delta - 8\dot{q}_2\rho\cos\alpha\cos\delta + 8\dot{q}_1\rho\cos\delta\sin\alpha \tag{24}$$

$$\frac{\partial\mathcal{D}}{\partial\dot{\delta}} = -8\dot{\delta}\rho^2 + 8\dot{q}_1\rho\cos\alpha\sin\delta + 8\dot{q}_2\rho\sin\alpha\sin\delta. \tag{25}$$

The non-linear behavior of $\mathcal{D}$ with respect to $\mathfrak{X}$ is now studied based upon a Monte Carlo (MC) sensitivity analysis. 1000 observation geometries are generated from an observatory at 20.710° inertial latitude and randomly chosen inertial longitude to a randomly generated object with semi-major axis / eccentricity / inclination bounds $a \in [15000\text{ km}, 45000\text{ km}]$, $e \in [0, 0.8]$, and $i \in$

$[0, 70^\circ]$, respectively. Objects with (periapsis altitude) $<$ 200 km and (apoapsis altitude) $>$ 60,000 km are rejected. All other orbital elements are chosen from a uniform distribution but constrained such that they appear at least 15° above the local horizon at the time of the observation. The latitude of the observatory corresponds to Haleakala, Maui, although any effects due to the altitude of the observatory are ignored. Dynamics are assumed to be point mass only and the Earth is assumed to rotate uniformly about the Earth centered inertial Z-axis.

We now derive an expression for the observation covariance matrix when the angle measurements are fit to a linear kinematic model at the tracklet epoch. A similar derivation is given in Maruskin, Scheeres, and Alfriend, but their derivation fits a quadratic kinematic model to the midpoint of the tracklet by making several simplifications [1]. In our case, we focus on extremely short tracklets where a linear model is sufficient. Suppose N image frames are included in a tracklet, where the frames are taken at times $t_0, t_1, \ldots, t_{N-1}$. To fit the right ascension $\alpha(t)$, say, to a linear model

$$\alpha(t_i) = \alpha_0 + \dot{\alpha}_0(t_i - t_0), \tag{26}$$

for $\mathbf{x}_0 = [\alpha_0, \dot{\alpha}_0]$, the partials $\tilde{H}_i$ are

$$\tilde{H}_i = \frac{\partial \alpha(t_i)}{\partial \mathbf{x}_0} = \begin{bmatrix} 1 & t_i - t_0 \end{bmatrix}. \tag{27}$$

As such, the information matrix Λ accumulated over all observations is

$$\Lambda = \sigma^{-2} \sum_{i=0}^{N-1} \tilde{H}_i^{\mathrm{T}} \tilde{H}_i = \sigma^{-2} \sum_{i=0}^{N-1} \begin{bmatrix} 1 & t_i - t_0 \\ t_i - t_0 & (t_i - t_0)^2 \end{bmatrix}, \tag{28}$$

where σ is the standard deviation of the measurement error. Now,

$$\sum_{i=0}^{N-1} 1 = N \tag{29}$$

$$\sum_{i=0}^{N-1} t_i - t_0 = \Delta t \sum_{i=0}^{N-1} i = \frac{N(N-1)\Delta t}{2} \tag{30}$$

$$\sum_{i=0}^{N-1} (t_i - t_0)^2 = \Delta t^2 \sum_{i=0}^{N-1} i^2 = \frac{N(N-1)(2N-1)\Delta t^2}{6}, \tag{31}$$

where $\Delta t = t_{N-1}/(N-1)$ is the time between frames. Substituting back into eq. (28) and taking the inverse, the covariance R is

$$R = \Lambda^{-1} = \sigma^2 \begin{bmatrix} \dfrac{2(2N-1)}{N(N+1)} & -\dfrac{6}{N(N+1)\Delta t^2} \\ -\dfrac{6}{N(N+1)\Delta t^2} & \dfrac{12}{N(N-1)(N+1)\Delta t^2} \end{bmatrix}. \tag{32}$$

In the current analysis, the tracklet length is set to $t_{N-1} = 4$ seconds with each tracklet containing $N = 5$ images spaced equally in time. For each of the 1000 observation geometries generated, 1000 instances of unbiased Gaussian measurement error are simulated separately for each variable in the tracklet based upon the corresponding variances in the covariance R derived above. That is, the

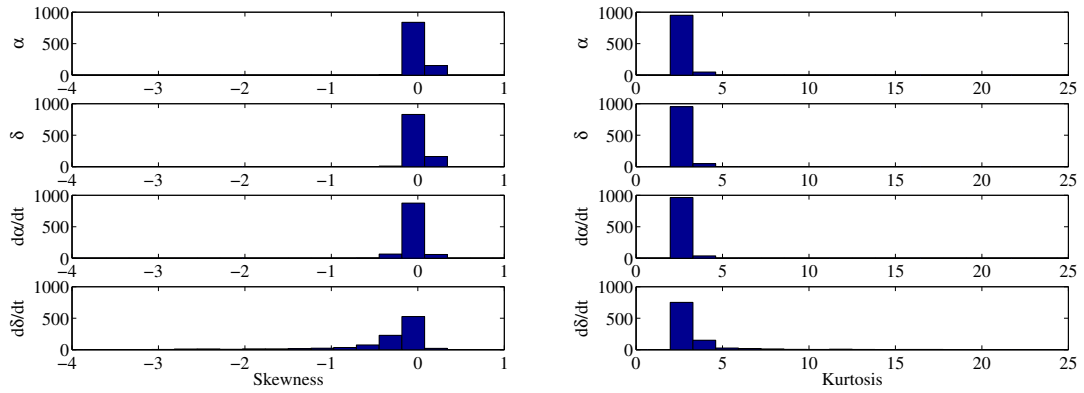

Figure 1. Histograms over all observation geometries sampled of the skewness (left) and kurtosis (right) of the discriminant distribution based on variations in a single variable in the tracklet.

measurement errors are assumed to be small enough such that the non-linear behavior of the energy is the sum of variations due to each individual component in the tracklet.

Figure 1 are histograms of the skewness and kurtosis of the energy distribution over all observation geometries sampled, separated by the variable to which noise is added in the tracklet. The range hypothesis is fixed to the true value of range as one is most interested in cases where the true range hypothesis is falsely eliminated. The energy remains nearly Gaussian (skewness ≈ 0, kurtosis ≈ 3) when α, δ, or $\dot{\alpha}$ are varied. The Jarque-Bera normality test corroborates this observation with less than 12% of sample orbits rejecting the null hypothesis (i.e., distribution is normal) with probability of false rejection $p < 0.05$, as seen in Figure 2. The p-value criterion indicates that one can expect at most 5% of the rejections to be due to random sampling error. The observed rejection rates, especially for the angle data, are consistent with this expectation. This property clearly does not hold, however, when $\dot{\delta}$ is varied, with 478 of the 1000 MC objects rejecting the null hypothesis with $p < 0.05$. Since $\delta \approx 0$ and $\dot{\delta} \approx 0$ for many objects in the orbit element bounds given, $\dot{\delta} \approx \dot{\delta}_{\mathcal{D},\max}$, and thus a linear approximation of $\mathcal{D}$ is inappropriate for such objects, as illustrated in an example in Figure 3. Nonetheless, errors in the tracklet are unlikely to overly increase $\mathcal{D}$ beyond the $+n_{\mathcal{D}}\sigma_{\mathcal{D}}$ upper bound determined linearly since non-linearities tend to skew the distribution negatively. Consequently, the hypothesis rejection criterion is modified as in eq. (18) in this paper with $n_{\mathcal{D}} = 3$ as false negative association outcomes are limited. The probability of missing an association due to measurement errors is at most 0.26998%.

Angular Momentum Magnitude Bound

Similar to the energy, the angular momentum magnitude h of an object may be related to a polynomial of range-rate

$$2\mathcal{E}h^2 = [\dot{\rho}^2 + w_1\dot{\rho} + F(\rho)][c_0\dot{\rho}^2 + P(\rho)\dot{\rho} + U(\rho)], \tag{33}$$

where $c_0 > 0$ is a coefficient determined by the input parameters, and $P(\rho)$ and $U(\rho)$ are functions of the range and input parameters. Thus, if eccentricity bounds $[e_{\text{MIN}}, e_{\text{MAX}}]$ are specified and if the quartic equation

$$2\mathcal{E}h^2\big|_{e=e_{\text{MAX}}} = -\mu^2(1 - e_{\text{MAX}}^2) = [\dot{\rho}^2 + w_1\dot{\rho} + F(\rho)][c_0\dot{\rho}^2 + P(\rho)\dot{\rho} + U(\rho)] \tag{34}$$

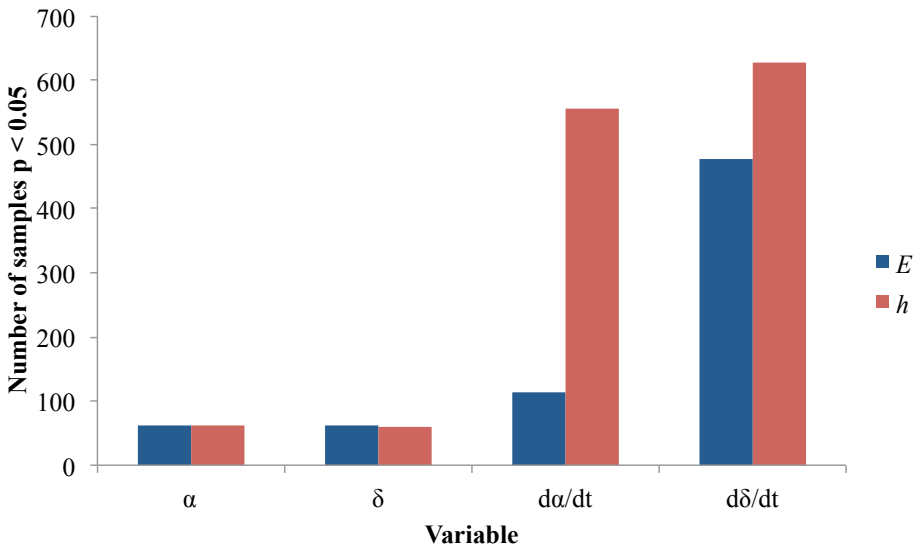

Figure 2. Number of observation geometry samples that reject the normality null hypothesis with $p < 0.05$ for the distribution in orbit energy (E) and angular momentum magnitude (h) when white noise is added to different variables in the tracklet.

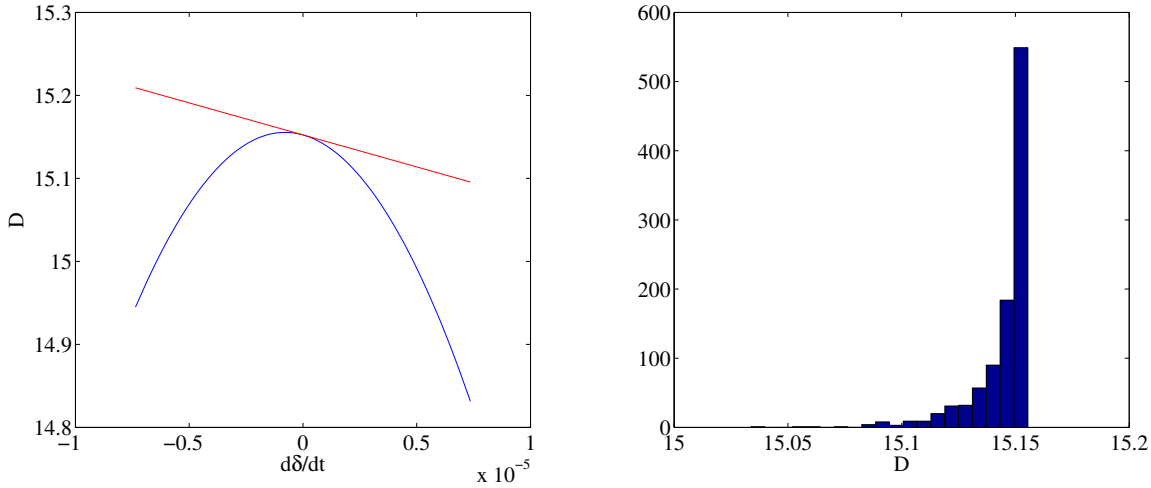

Figure 3. (Left) The blue line indicates the value of discriminant $\mathcal{D}$ as a function of the variation in declination time derivative $\dot{\delta}$ for one observation geometry sample. The red line is the linear approximation at the reference point. Values plotted for ± 6 standard deviations in $\dot{\delta}$. (Right) Histogram of $\mathcal{D}$ for 1000 Monte Carlo samples of $\dot{\delta}$ from a Gaussian distribution for the same observation geometry. Skewness = -2.6946, kurtosis = 13.271, and $p < 0.001$ for the Jarque-Bera normality test.

does not have a real solution, the range hypothesis cannot be true and is subsequently eliminated. Note that it is not necessary to check the case for e_{MIN} as $-\mu^2(1-e_{\mathrm{MIN}}^2) \leq -\mu^2(1-e_{\mathrm{MAX}}^2)$. Instead of examining the discriminant of this quartic equation, the minima of

$$G(\dot{\rho};\rho) = [\dot{\rho}^2 + w_1\dot{\rho} + F(\rho)][c_0\dot{\rho}^2 + P(\rho)\dot{\rho} + U(\rho)] + \mu^2(1-e_{\mathrm{MAX}}^2) \tag{35}$$

$$= c_0\dot{\rho}^4 + (P+c_0w_1)\dot{\rho}^3 + (U+c_0F+w_1P)\dot{\rho}^2 + (PF+w_1U)\dot{\rho} + UF + \mu^2(1-e_{\mathrm{MAX}}^2) \tag{36}$$

is analytically solved for, where the semi-colon indicates that ρ is hypothesized and may be assumed as known. Viewed as a function of the angle-rates, G is similarly a quartic polynomial. For there to be a real solution, there must exist some $\dot{\rho} = \dot{\rho}_m$ that satisfies

$$G(\dot{\rho} = \dot{\rho}_m;\rho) \equiv G_m < 0 \tag{37}$$

$$\left.\frac{\mathrm{d}G}{\mathrm{d}\dot{\rho}}\right|_{\dot{\rho}=\dot{\rho}_m} = 0 \tag{38}$$

$$\left.\frac{\mathrm{d}^2G}{\mathrm{d}\dot{\rho}^2}\right|_{\dot{\rho}=\dot{\rho}_m} > 0. \tag{39}$$

Note that the minimum value that $2\mathcal{E}h^2$ can take is $-\mu^2(1-0^2) = -\mu^2$, meaning that G_m is bounded from below by $-\mu^2 + \mu^2(1-e_{\mathrm{MAX}}^2) = -\mu^2 e_{\mathrm{MAX}}^2$.

Similar to the energy, one is interested in whether the variance of G_m may again be computed as

$$\sigma_{G_m}^2 = \left[\frac{\partial G_m}{\partial \mathfrak{X}}\right] R \left[\frac{\partial G_m}{\partial \mathfrak{X}}\right]^{\mathrm{T}}. \tag{40}$$

The criterion for range hypotheses consistent with the angular momentum bounds may be modified so that, if

$$G_m - n_{G_m}\sigma_{G_m} > 0, \tag{41}$$

then the range hypothesis is eliminated with some level of confidence specified by n_{G_m}. It is computationally intractable to compute the partials analytically; in this paper, a numerical derivative is taken via central difference. Figure 4 are histograms of the skewness and kurtosis of the distribution of G_m over all observation geometries sampled, separated by the variable to which noise is added in the tracklet. G_m remains nearly Gaussian when α or δ are varied but not for $\dot{\alpha}$ or $\dot{\delta}$; refer to Figure 2 for the results of the Jarque-Bera normality test. The linear approximation again becomes inappropriate for certain objects due to the observed angle-rate values being in the proximity of local extrema of G_m. Variations in $\dot{\alpha}$ skew the G_m distribution positively, indicating that the distribution is non-linearly deformed due to a local minimum. On the other hand, variations in $\dot{\delta}$ skew the G_m distribution in both signs, indicating that it is deformed by both local minima and maxima: Figures 5 and 6 are two illustrative examples.

Errors in $\dot{\alpha}$ are unlikely to overly decrease G_m beyond the $-n_{G_m}\sigma_{G_m}$ bounds determined linearly, as can be deduced from Figure 6, limiting false negative association outcomes. Consequently, the hypothesis rejection criterion is modified as in eq. (41) in this paper for the α, δ, and $\dot{\alpha}$ directions with $n_{G_m} = 3$. Then, the probability of missing an association due to measurement errors is at most 0.26998%. The same cannot be said, however, of $\dot{\delta}$ when the distribution of G_m is negatively skewed, so the following non-linear criterion is implemented. Recall that G_m is a quartic polynomial in $\dot{\delta}$ given the hypothesized value of ρ and $\dot{\rho} = \dot{\rho}_m$. Probability is a conserved quantity in the map between $\dot{\delta}$ and G_m as this map is one-to-one and continuously differentiable; e.g., if values of

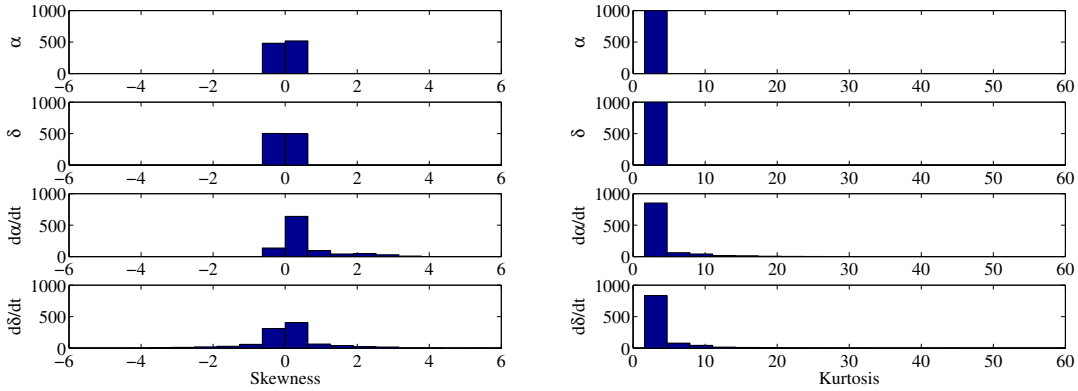

Figure 4. Histograms over all observation geometries sampled of the skewness (left) and kurtosis (right) of the G_m distribution based on variations in a single variable in the attributable vector.

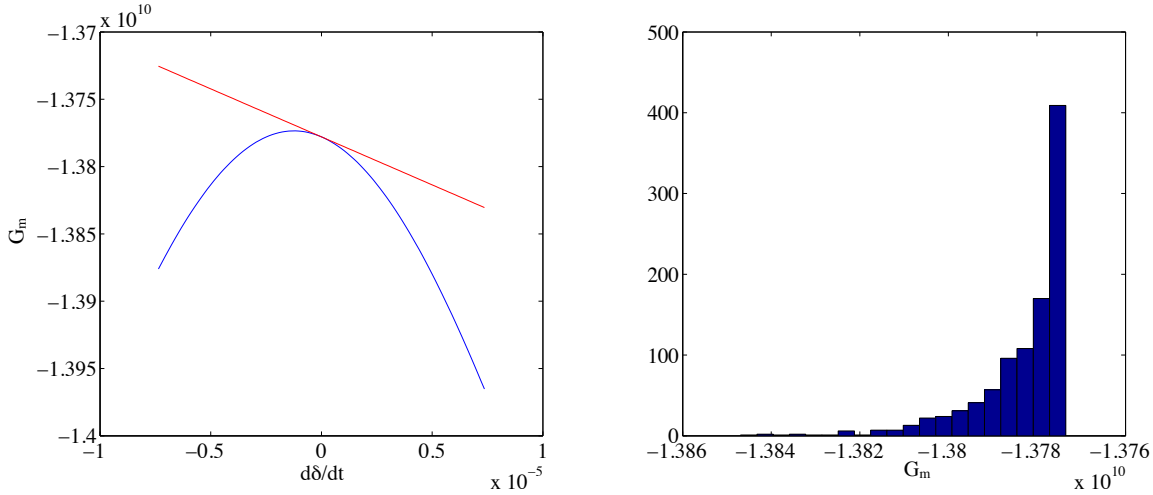

Figure 5. (Left) The blue line indicates the value of discriminant G_m as a function of the variation in declination time derivative $\dot{\delta}$ for one observation geometry sample. The red line is the linear approximation at the reference point. Values plotted for $\pm$6 standard deviations in $\dot{\delta}$. (Right) Histogram of G_m for 1000 Monte Carlo samples of $\dot{\delta}$ from a Gaussian distribution for the same observation geometry. Skewness = -2.0274, kurtosis = 8.317, and $p < 0.001$ for the Jarque-Bera normality test.

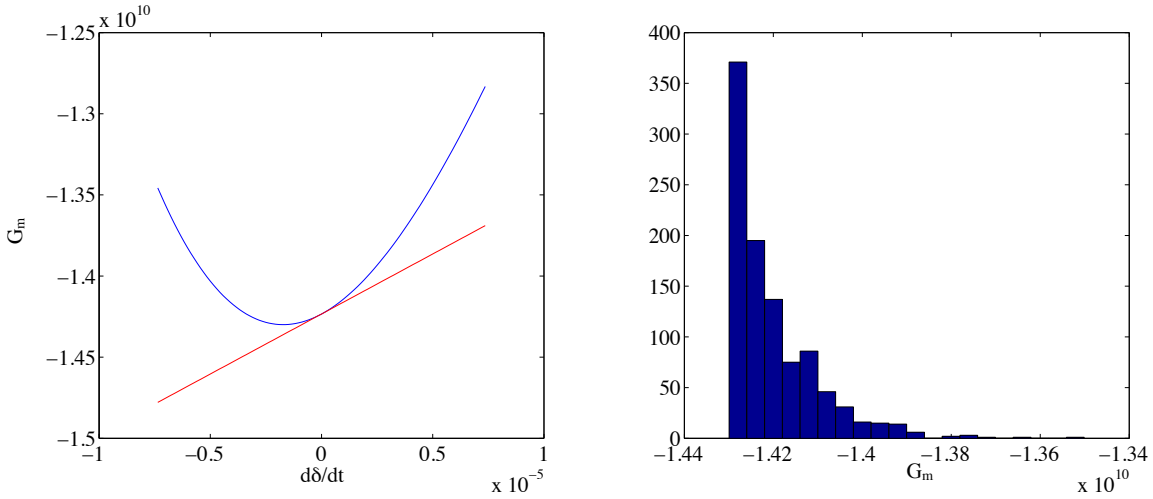

Figure 6. (Left) The blue line indicates the value of discriminant G_m as a function of the variation in declination time derivative $\dot{\delta}$ for one observation geometry sample. The red line is the linear approximation at the reference point. Values plotted for $\pm$6 standard deviations in $\dot{\delta}$. (Right) Histogram of G_m for 1000 Monte Carlo samples of $\dot{\delta}$ from a Gaussian distribution for the same observation geometry. Skewness = 1.8387, kurtosis = 8.0159, and $p < 0.001$ for the Jarque-Bera normality test.

$\dot{\delta}$ up to $\pm 3\sigma_{\dot{\delta}}$ are considered in the analysis, then 99.730% of outcomes in G_m are accounted for. As such, a range hypothesis is eliminated with some specified level of confidence specified by $n_{\dot{\delta}}$ if

$$\min\left[G_m(\dot{\delta}+n_{\dot{\delta}}\sigma_{\delta}), G_m(\dot{\delta}-n_{\dot{\delta}}\sigma_{\delta}), G_m(\dot{\delta}_{E_1}), G_m(\dot{\delta}_{E_2}), G_m(\dot{\delta}_{E_3})\right] > 0, \tag{42}$$

where $\dot{\delta}_{E_i}$ $(i = 1, 2, 3)$ are values of $\dot{\delta}$ that correspond to local extrema of G_m with respect to $\dot{\delta}$. In this paper, $n_{\dot{\delta}} = n_{G_m} = 3$.

Angular Momentum Direction Bound

The angular momentum vector $\boldsymbol{h}$ may be written as a function of range-rate as

$$\boldsymbol{h} = \dot{\rho}\boldsymbol{h}_1 + \boldsymbol{H}(\rho, \mathfrak{X}), \tag{43}$$

where $\boldsymbol{H}$ consolidates all terms which are not direct functions of range-rate. Since $\mathbf{H}$ may be computed solely based on the input and hypothesized variables, if one can approximate $\boldsymbol{h} \approx \boldsymbol{H}$ with sufficient accuracy, then this approximation may be used to eliminate range hypotheses. For a given tracklet $\mathfrak{X}$, the directional error $\Delta\theta_h$ between $\boldsymbol{h}$ and $\boldsymbol{H}$ is maximum when $\boldsymbol{h}_1 \perp \boldsymbol{H}$ such that

$$\Delta\theta_h = \arccos\left[\frac{\boldsymbol{h}\cdot\boldsymbol{H}}{hH}\right] = \arccos\left[\left\{\left(\frac{\dot{\rho}h_1}{H}\right)^2 + 1\right\}^{(-1/2)}\right]. \tag{44}$$

A MC simulation is conducted to ascertain if and when the above approximation is appropriate. Here, 10^6 observations are simulated, each of objects randomly generated based on the distribution of objects in the Joint Space Operations Center (JSpOC) public catalog. The semi-major axis (a) / eccentricity (e) / inclination (i) of cataloged objects that meet the same bounds as the MC analysis

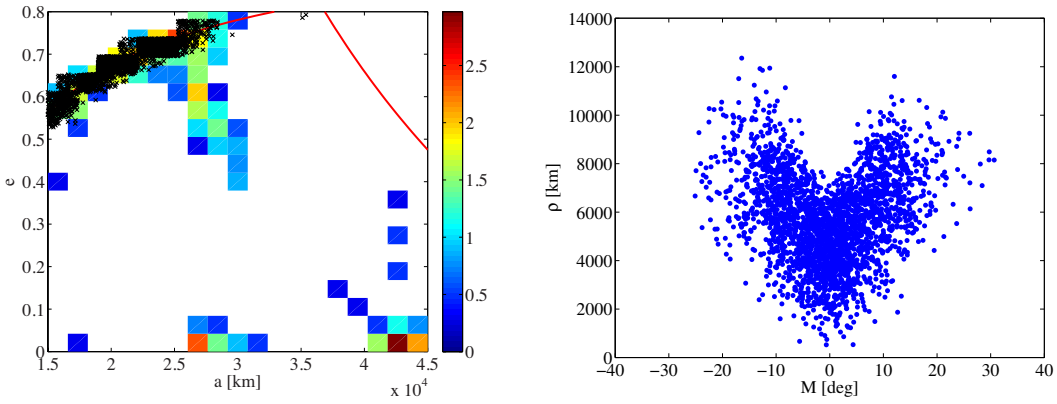

Figure 7. (Left) Black x's represent the distribution of Monte Carlo samples for which the approximation $\boldsymbol{h} \approx \boldsymbol{H}$ deviates by more than 30° in direction in the semi-major axis a / eccentricity e space. Color map is the $\log_{10}$ of the number of public JSpOC catalogued objects that reside in each discretization bin. (Right) Distribution of the same Monte Carlo samples in the topocentric range ρ / mean anomaly M space.

in the previous sections are separated into a $20 \times 20 \times 20$ discretization grid. The number of cataloged objects that reside in each bin defines a density function in this discretized space from which MC samples are taken. A uniform distribution is assumed over each discretization bin as well as over the remaining orbital elements. Measurement parameters such as the observer location are the same as in the previous example. For 99.731% of MC samples, $\boldsymbol{H}$ was within 30 degrees of $\boldsymbol{h}$, or $\Delta\theta_h \leq 30°$; Figure 7 represents the distribution of samples for which the approximation was worse ($\Delta\theta_h > 30°$) in several state spaces. We expect that $\boldsymbol{h} \approx \boldsymbol{H}$ is poor when $\dot{\rho}$ is large. Indeed, all of the poorly approximated samples are highly eccentric and observed near their periapses.

We may compare the approximated angular momentum direction to the specified inclination bounds $[i_{\min}, i_{\max}]$ or to the angular momentum direction computed using a range / range hypothesis pair (ρ_1, ρ_2) for tracklets $\mathfrak{X}_1$ and $\mathfrak{X}_2$

$$\boldsymbol{h} \propto [\boldsymbol{r}_1(\rho_1, \mathfrak{X}_1) \times \boldsymbol{r}_2(\rho_2, \mathfrak{X}_2)]\,, \tag{45}$$

where $\boldsymbol{r}_1$ and $\boldsymbol{r}_2$ are position vectors of the hypothesized objects. The latter is implemented for this work based on the MC analysis such that, given a pair of tracklets, if the hypothesized range for both is greater than 15,000 km AND if the approximated angular momentum vector differs in direction from that computed based on the hypothesized position vectors by more than 30°, then that pair of range hypotheses is regarded as inconsistent with information from the actual observation and is thus discarded. Assuming that the MC samples are an accurate representation of the distribution of measurements made of MEO, GEO, and HEO objects, by fitting the MC results to a binomial distribution, the 95% confidence interval for the probability of a missed association is $0\% \sim 0.00036889\%$.

RESULTS

The above formulation is tested upon simulated optical observations of objects in MEO, HEO, and GEO. Observations are taken for a subset of 100 objects in the public JSpOC catalogue. These objects appear at least 15° above the local horizon at epoch and move slower than 0.01° /sec instantaneously in both right ascension and declination at epoch. Figure 8 is a graphical representation of

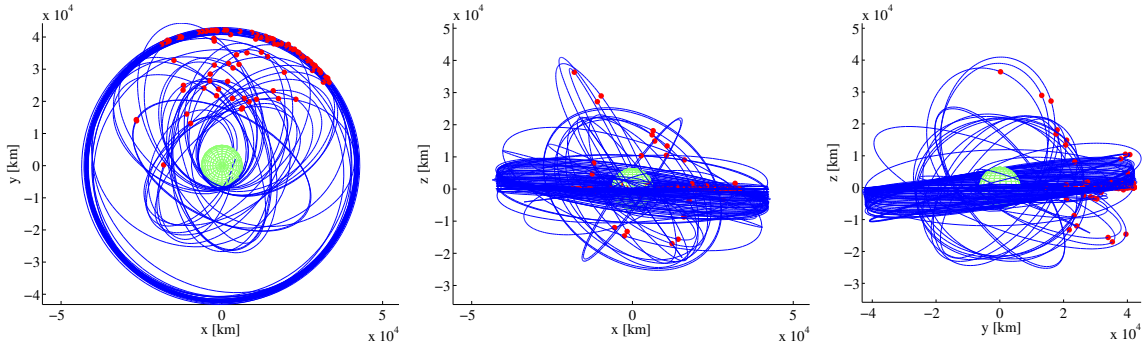

Figure 8. The orbits of all 100 objects generated in this simulation in an Earth centered inertial coordinate system. The red points indicate position at epoch. The green sphere is the Earth.

the MC sample objects at epoch. Every 30 seconds, a virtual telescope centers its $1^\circ \times 1^\circ$ field of view (FOV) on a randomly chosen object. All objects that fall within this FOV are simultaneously observed. The observatory is located at the inertial latitude of Haleakala and 0° inertial longitude at epoch. Tracklet lengths are chosen to be either 2 seconds or 4 seconds, each with 5 images spaced equally in time. A total of 836 tracklets are generated. For each of the possible $\binom{836}{2} = 349{,}030$ tracklet pair combinations, a 100×100 range / range hypothesis pair set is generated based on the same orbital element bounds as all previous analyses

$$a \in [15000 \text{ km}, 45000 \text{ km}], e \in [0, 0.8], i \in [0, 70^\circ]. \tag{46}$$

These range / range hypotheses are then evaluated as described in the previous sections. Additionally, for range / range hypotheses that remain, a Lambert problem solution is differentially corrected to their corresponding angle observations using a batch formulation of the UKF. Range / range hypotheses resulting in a ± 3-σ residual root mean square (RMS) or greater are rejected. Tracklet pairs with zero range / range hypotheses remaining are deemed unassociated.

We first consider a tracklet length of 4 seconds. The plot on the left in Figure 9 is a color map of the number of range / range hypotheses that remain for all possible tracklet pairs after applying the gating method by Schumacher et al.; that is, the color of the cell located at (X, Y) represents the $\log_{10}$ of the number of remaining hypotheses when the X-th tracklet and the Y-th tracklet measured that night are paired. On the right is a histogram of the number of remaining range / range hypotheses over all possible tracklet pairs. Similar plots are given for when angle-rate information is added (Figure 10) and when the solutions are further differentially corrected (Figure 11). A summary of results for both the 4 second and 2 second tracklet cases is given in Table 1. The proposed method, simply based on bounds on constants of motion, is able to deem over to 30% of the tracklet pair sets as unassociated regardless of tracklet length; a more than 900 fold improvement over the baseline based on only angular information. More importantly, no associations are missed. In addition, from the batch UKF results, the BVP formulation of AR IOD shows promise of being a feasible alternative to its IVP counterpart for extremely short tracklets in terms of its low missed association rates. Efficient prefiltering as demonstrated in this paper is critical for the BVP formulation to be attractive computationally.

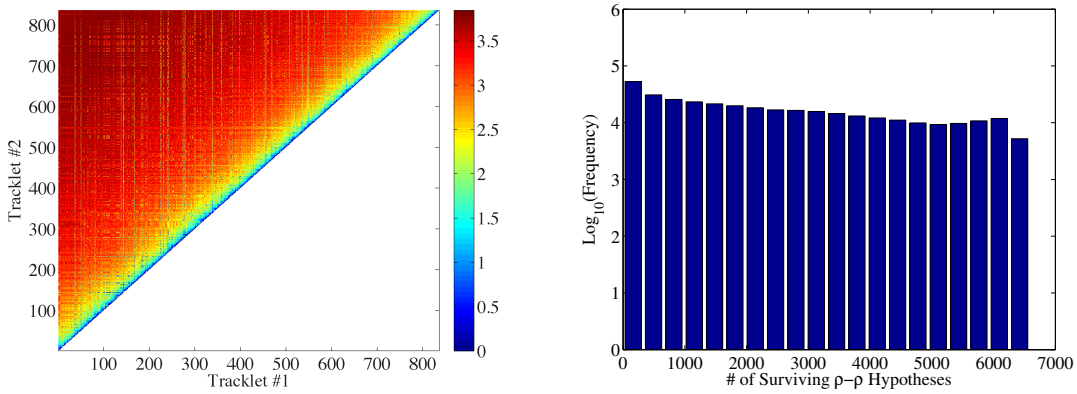

Figure 9. (Left) Number of remaining range / range hypotheses for all valid combinations of tracklet pairs when only angular information is used for gating. Colors scaled in $\log_{10}$. (Right) Histograms of the number of remaining range / range hypotheses for all tracklet pairs processed. Tracklet length is 4 seconds with 5 images.

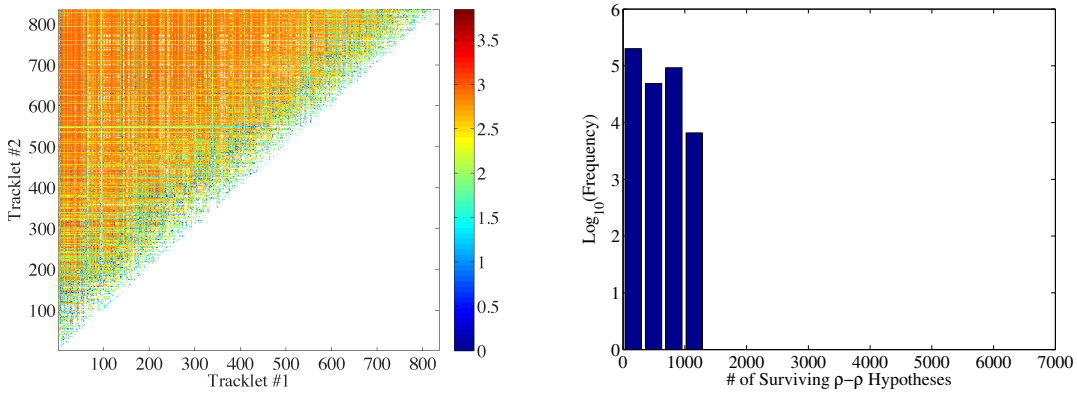

Figure 10. (Left) Number of remaining range / range hypotheses for all valid combinations of tracklet pairs when both angle and angle-rate information is used for gating. Colors scaled in $\log_{10}$. (Right) Histograms of the number of remaining range / range hypotheses for all tracklet pairs processed. Tracklet length is 4 seconds with 5 images.

Table 1. Summary of tracklet association results based on the method employed. "n sec" indicates results for the proposed method for the specified tracklet length. Median number of remaining hypotheses shown only for tracklet pairs which are deemed associated. "Missed" association indicates a false negative outcome.

	Baseline	**4 sec**	**2 sec**	**4 sec + UKF**
% of tracklets deemed unassociated	0.036114%	33.9892%	33.7966%	73.5002%
Median # of remaining hypotheses	1982	595	601	112
# of missed association outcomes	0	0	0	0

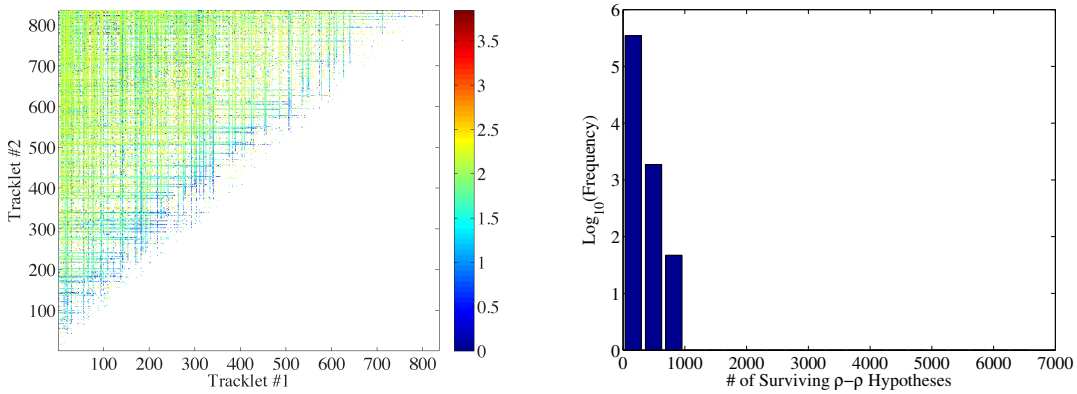

Figure 11. (Left) Number of remaining range / range hypotheses for all valid combinations of tracklet pairs when both angle and angle-rate information is used for gating. Lambert's problem is solved based on the remaining hypotheses and differentially corrected with a batch formulation of the unscented Kalman filter. Colors scaled in $\log_{10}$. (Right) Histograms of the number of remaining range / range hypotheses for all tracklet pairs processed. Tracklet length is 4 seconds with 5 images.

CONCLUSION

In this paper, methods are proposed to improve the computational efficiency of a boundary value problem formulation of initial orbit determination via admissible regions. Both angles and angles-rate information from extremely short-arc optical tracks, potentially only a few seconds long, are used to bound the constants of motion for some hypothesized object. These bounds act as criteria to allow one to eliminate hypotheses that are physically infeasible before a more computationally costly Lambert solver or differential corrector is applied. The linearity of maps between measurement errors and errors in the constants of motion are studied so that missed associations are minimized. Processing simulated observations of various medium Earth, high Earth, and geosynchronous orbit objects, the proposed criteria by itself succeeded in eliminating 40% of all possible track parings with 0 missed associations. Future work is to expand gating methodologies to initial orbit determination algorithms that take three or more tracklets as input.

ACKNOWLEDGEMENTS

This research was supported by AFOSR grant FA9550-11-1-0188.

REFERENCES

[1] J. M. Maruskin, D. J. Scheeres, and K. T. Alfriend, "Correlation of optical observations of objects in earth orbit," *Journal of Guidance, Control and Dynamics*, Vol. 32, No. 1, 2009, pp. 194–209.

[2] G. Tommei, A. Milani, and A. Rossi, "Orbit determination of space debris: admissible regions," *Celestial Mechanics and Dynamical Astronomy*, Vol. 97, 2007, pp. 289–304.

[3] D. Farnocchia, G. Tommei, A. Milani, and A. Rossi, "Innovative methods of correlation and orbit determination for space debris," *Celestial Mechianics and Dynamical Astronomy*, Vol. 107, No. 1-2, 2010, pp. 169–185.

[4] A. Milani, G. Tommei, D. Farnocchia, A. Rossi, T. Schildknecht, and R. Jehn, "Correlation and orbit determination of space objects based on sparse optical data," *Mon. Not. R. Astron. Soc.*, Vol. 417, 2012, pp. 2094–2103.

[5] K. J. DeMars and M. K. Jah, "Probabilistic Initial Orbit Determination Using Gaussian Mixture Models," *Journal of Guidance, Control, and Dynamics*, Vol. 36, No. 5, 2013, pp. 1324–1335.

[6] J. A. Siminski, O. Montenbruck, H. Fiedler, and M. Weigel, "Best Hypothesis Search on Iso-Energy-Grid for Initial Orbit Determination and Track Association," 2013. Presented at the *23rd AAS/AIAA Spaceflight Mechanics Meeting*, Kauai, HI. AAS 13-239.

[7] K. Fujimoto and D. J. Scheeres, "Correlation of Optical Observations of Earth-Orbiting Objects and Initial Orbit Determination," *Journal of Guidance, Control, and Dynamics*, Vol. 35, No. 1, 2012, pp. 208–221.

[8] J. L. I. Worthy, M. J. Holzinger, and K. Fujimoto, "Optical Sensor Constraints on Space Object Detection and Admissible Regions," 2013. Presented at the *2013 AAS/AIAA Astrodynamics Specialist Conference*, August 11 - 15, 2013, Hilton Head, SC.

[9] A. Milani, G. Gronchi, M. Vitturi, and Z. Knežević, "Orbit Determination with Very Short Arcs. I Admissible Regions," *Celestial Mechanics and Dynamical Astronomy*, Vol. 90, 2004, pp. 57–85.

[10] A. Milani, G. Gronchi, Z. Knežević, M. E. Sansaturio, and O. Arratia, "Orbit Determination with Very Short Arcs II. Identifications," *Icarus*, Vol. 179, 2005, pp. 350–374.

[11] A. Milani and Z. Knežević, "From Astrometry to Celestial Mechanics: orbit determination with Very short arcs," *Celestial Mechanics and Dynamical Astronomy*, Vol. 92, 2005, p. 118.

[12] P. W. Schumacher, Jr., M. Wilkins, and C. Roscoe, "Parallel Algorithm for Track Initiation for Optical Space Surveillance," 2013. Presented at the *6th European Conference on Space Debris*, Darmstadt, Germany.

[13] J. Virtanen, K. Muinonen, and E. Bowell, "Statistical Ranging of Asteroid Orbits," *Icarus*, Vol. 154, 2001, pp. 412–431.

[14] J. A. Siminski, O. Montenbruck, H. Fiedler, and T. Schildknecht, "Short-Arc Tracklet Association for Geostationary Objects," *Advances in Space Research*, 2014. In press.

[15] S. M. Gadaleta, J. T. Horwood, and A. B. Poore, "Short Arc Gating in Multiple Hypothesis Tracking for Space Surveillance," 2012. Proc. SPIE 8385, 83850Y.

[16] D. Vallado, *Fundamentals of Astrodyamics and Applications*. Hawthorne, CA: Microcosm Press, third ed., 2007.

[17] R. H. Battin, *An Introduction to the Mathematics and Methods of Astrodynamics*. Reston, VA: American Institute of Aeronautics and Astronautics, Inc., revised ed., 1999.